Pis'ma v ZhETF, vol. 89, iss. 2, pp. 70 – 74 © 2009 January 25

Terahertz laser based on optically pumped graphene: model and feasibility of realization

V. Ya. Aleshkin, A. A. Dubinov, V. Ryzhii[+*]

Institute for Physics of Microstructures RAS, 603950 Nizhny Novgorod, Russia

[+] *University of Aizu, 965-8580 Aizu-Wakamatsu, Japan*

[*] *Japan Science and Technology Agency, CREST, 107-0075 Tokyo, Japan*

Submitted 13 November 2008

We consider a terahertz laser based on optically pumped graphene layer and bilayer as the active media and suggested waveguide structure. Using the developed model, we calculate the spectral dependences the dynamic conductivity of the optically pumped graphene layer and bilayer associated with the interband and intraband transitions, estimate the pumping optical power required for lasing, and demonstrate the feasibility of realization of such a laser.

PACS: 78.66.–w, 81.05.Uw

Recent progress in formation of different graphene-based structures not only by pealing method but also by various epitaxial techniques indicates that exceptional electronic and mechanical properties of graphene can utilized in real nanoelectronic and nanoelectromechanical devices. Graphene structures can also be used in optoelectronics devices such as photodetectors, modulators, and sources of longwavelength radiation. Due to the gapless energy spectrum in graphene and rather small energy gaps in graphene nanoribbons and graphene bilayers, such optoelectonic devices can operate in the terahertz (THz) range of spectrum. As shown [1, 2] (see also [3, 4]), the optically pumped graphene (in which the photoexcited electrons and holes are concentratied near the bottom of the conduction band and the top of the valence band due to emission of the cascade of optical phonons) can exhibit negative dynamic THz conductivity associated with the population inversion and domination of the interband emission over the intraband Drude absorption [1, 4]. This can be used for creation of lasers generating THz electromagnetic radiation. However, the crucial point in realization of a graphene THz laser is the feasibility of a waveguide system which could provide sufficiently low loses of THz radiation. In this paper, we consider a graphene THz laser with optical pumping which includes a graphene layer or graphene bilayer and a waveguide system using the developed model. The latter consists of a thinned Si substrate of thickness $10-50\,\mu$m with Au film on one side and a SiO_2 layer of thickness 300 nm on the other followed by 80 nm SiC layer. The graphene layer is sandwiched between the SiC layer and 300 nm layer of SiO_2. This structure (see Fig.1) is akin to that fabricated in Ref. [5]. Under optical excitation, electrons and holes are photogenerated with the energy $\varepsilon_0 = \hbar\Omega/2$. Here $\hbar\Omega$ is the energy of the incident photons. The electron-electron and electron-phonon interactions thermalize the distributions of photogenerated electrons and holes. So the electron and hole energy distributions are close to the Fermi distributions with quasi-Fermi energies $F > 0$. We shall use this simplified distributions for conductivity estimations. Note that the electron and hole distribution functions, $f_e(\varepsilon)$ and $f_h(\varepsilon)$, exceed 1/2 in certain energy ranges near the bottom of the conduction band and the top of the valence band, i.e., relatively small ε. This implies the population inversion of the states in these energy ranges.

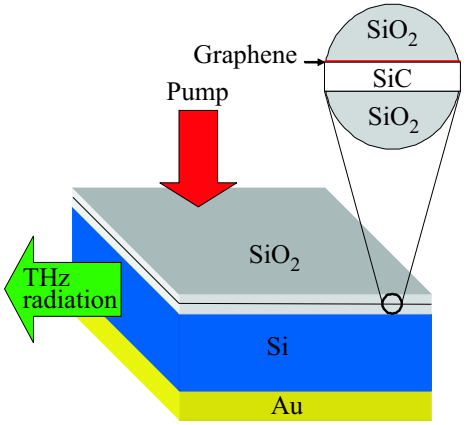

Fig.1. Schematic view of the device structure

In the optically pumped ungated and undoped graphene the equilibrium electron and hole densitiess, n and p, are equal to each other ($n = p$), the Fermi distributions of electrons and holes are characterized by

the same Fermi energy F and the effective temperature T, i.e.,

$$f_e(\varepsilon) = f_h(\varepsilon) = \left[1 + \exp\left(\frac{\varepsilon - F}{k_B T}\right)\right]^{-1}, \qquad (1)$$

where k_B is the Boltzmann constant. For simplicity we disregard the difference between the electron (hole) and lattice temperatures.

The real part of the dynamic conductivity $\mathrm{Re}\,\sigma_\omega$ of a non-equilibrium electron-hole system in graphene, which determines the absorption coefficient of photons with the frequency ω, comprises the contributions of both the interband and intraband transitions:

$$\mathrm{Re}\,\sigma_\omega = \mathrm{Re}\,\sigma_\omega^{\mathrm{inter}} + \mathrm{Re}\,\sigma_\omega^{\mathrm{intra}}. \qquad (2)$$

Taking into account that the graphene band structure includes two nonequivalent valleys in the K points of the Brillouin zone and the spin degeneracy, as well as considering that the value of the interband momentum matrix element is equal to $v_W m_0$ (where m_0 is the free electron mass, $v_W \simeq 10^8$ cm/s is the characteristic velocity of electrons and holes in graphene), one can derive the following formula for the interband conductivity:

$$\mathrm{Re}\,\sigma_\omega^{\mathrm{inter}} = \frac{e^2}{2\hbar}\left[1 - f_e\left(\frac{\hbar\omega}{2}\right) - f_h\left(\frac{\hbar\omega}{2}\right)\right] =$$

$$= \frac{e^2}{2\hbar}\tanh\left(\frac{\hbar\omega - 2F}{4k_B T}\right). \qquad (3)$$

The analogous expression for a graphene bilayer can be presented as

$$\mathrm{Re}\,\sigma_\omega^{\mathrm{inter}} = \frac{e^2\,(\hbar\omega + 2\gamma_1)}{4\hbar\,(\hbar\omega + \gamma_1)}\tanh\left(\frac{\hbar\omega - 2F}{4k_B T}\right), \qquad (4)$$

where $\gamma_1 \approx 0.4$ eV is band parameter [6]. To derive Eq.(4) we have used the follow electron spectrum in the nearest bands $\varepsilon(p) = \pm\left(-\gamma_1 + \sqrt{4v_0^2 p^2 + \gamma_1^2}\right)/2$ [6]. Note that for graphene bilayer the interband matrix element of the momentum operator equals $\langle\psi_c|p_x|\psi_v\rangle = 2i\varepsilon(p)m_0 v_W^2 p_y/[v_W^2 p^2 + \varepsilon(p)^2]$.

For $\mathrm{Re}\,\sigma_\omega^{\mathrm{intra}}$ one can use the Drude formula

$$\mathrm{Re}\,\sigma_\omega^{intra} = 2e\mu n/(1 + \omega^2\tau^2). \qquad (5)$$

Here e is the electron charge, μ is the electron and hole mobility in graphene, τ is the momentum relaxation time of electrons and holes associated with their scattering, $\hbar$ is the Planck constant, and n is the electron concentration in the conduction band:

$$n = \frac{2}{\pi\hbar^2 v_W^2}\int_0^\infty \frac{\varepsilon\, d\varepsilon}{1 + \exp\left(\frac{\varepsilon - F}{k_B T}\right)}, \qquad (6)$$

$$n = \frac{2}{\pi\hbar^2 v_W^2}\int_0^\infty \frac{(\varepsilon + \gamma_1/2)\, d\varepsilon}{1 + \exp\left(\frac{\varepsilon - F}{k_B T}\right)}, \qquad (7)$$

where Eqs. (6) and (7) are valid for graphene and graphene bilayer, respectively.

Figure 2a shows the real part of the dynamic conductivity $\mathrm{Re}\,\sigma_\omega$ as a function of the photon energy $\hbar\omega$

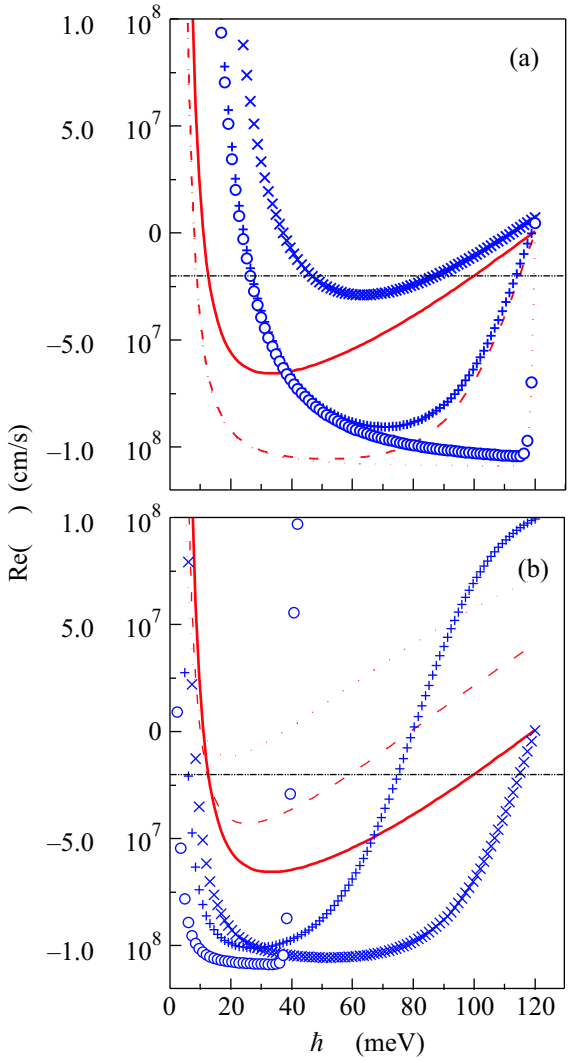

Fig.2. Real part of the dynamic conductivity $\mathrm{Re}\sigma_\omega$ vs photon energy $\hbar\omega$ of a graphene layer (a) for different temperatures and mobilities at $F = 60$ meV and (b) for different temperatures and different Fermi energies at $\mu = 2\cdot 10^5$ cm^2/Vs.

calculated for the Fermi energy $F = 60$ meV at three values of the temperature ($T = 4.2$, 77 and 300 K) and two values of the electron and hole mobility ($\mu = 2\cdot 10^5$ [7] and $2\cdot 10^4$ cm^2/Vs [8]). The momentum relaxation time was assumed to be $\tau = 10^{-12}$ s and 10^{-13} s [8], respectively. The same dependencies but calculated for dif-

ferent Fermi energies in the range $F = 20$–60 meV at $T = 77$ and 300 K and $\mu = 2 \cdot 10^5$ are demonstrated in Fig.2b. As seen from Fig.2, the width of the range of the photon energies where the real part of the dynamic conductivity $\mathrm{Re}\,\sigma_\omega < 0$ increases with decreasing temperature. Apart from this, the absolute value of $\mathrm{Re}\,\sigma_\omega$, i.e., $|\mathrm{Re}\,\sigma_\omega|$ also increases when the temperature drops. In particular, when $F = 60$ meV, $T = 300$ K, and $\mu = 2 \cdot 10^5$ cm^2/Vs, one obtains $\mathrm{Re}\,\sigma_\omega < -2 \cdot 10^7$ cm/s. As shown in the following, the latter value of $\mathrm{Re}\,\sigma_\omega$ is quite sufficient to achieve the stimulated emission in the graphene device with the waveguide under consideration for the TM mode. An increase in the mobility leads to the modification of the $\mathrm{Re}\,\sigma_\omega$ versus $\hbar\omega$ dependence similar to the modification of this dependence with decreasing temperature.

Figure 3 represents similar conductivity calculated for the bilayer graphene. From comparison Fig.2 and Fig.3 one can see that the single graphene layer is preferable for room temperature operation (see, however, below). This is associated with greater free carrier absorption in the graphene bilayer due to greater electron (and hole) concentration. The latest is the consequence of a higher density of low energy states in comparison with a monolayer graphene.

The spatial distributions of the electric field of the TE_0 and TM_0 modes and the refractive index for frequency $\omega/2\pi = 2$ THz are shown in Fig.4a. The Si layer width was chosen to provide the minimal generation threshold of these modes. For the calculation of the TE mode, Maxwell's equations could be presented in following form (in the coordinate system where the direction of the x axis coincides with the wave propagation direction and the direction of the z axis coincides with the structure growth direction):

$$\frac{d^2E_y(z)}{dz^2} + \left[\frac{\eta(z,\omega)^2\omega^2}{c^2} - k_x^2\right] E_y(z) = 0, \qquad (8)$$

where $E_y(z)$ is the amplitude of the y-th component of the electric field $E_y(\mathbf{r},t) = E_y(z)\exp(ik_x x - i\omega t)$ in the TE mode, η is the complex refractive index, k_x is the wave vector of the TE mode, c is the speed of light in vacuum. The quantities $E_y(z)$ and $\mathrm{d}E_y(z)/\mathrm{d}z$ are continuos at the interface between the layers with different refractive indices. The boundary conditions for the guided modes correspond to the conditions $E_y(z)\to 0$ for $z\to\pm\infty$. The amplitude $H_y(z)$ of y-th component of the magnetic field $H_y(\mathbf{r},t) = H_y(z)\exp(ik_x x - i\omega t)$ in the TM mode obeys the following equation:

$$\eta(z,\omega)^2\frac{d}{dz}\left(\frac{1}{\eta(z,\omega)^2}\frac{dH_y(z)}{dz}\right) +$$

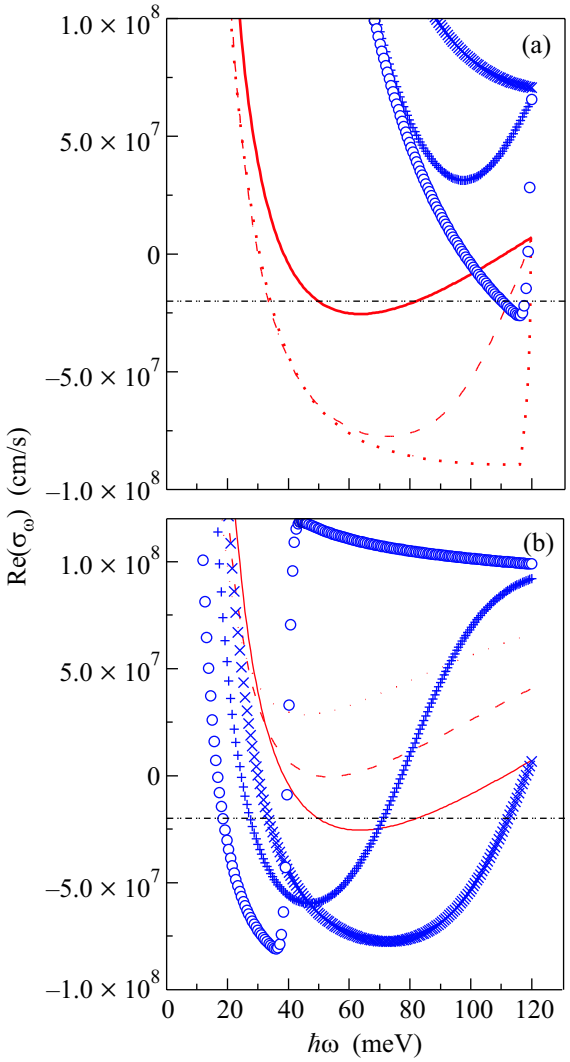

Fig.3. Real part of the dynamic conductivity $\mathrm{Re}\sigma_\omega$ vs photon energy $\hbar\omega$ of a graphene bilayer (a) for different temperatures and mobilities at $F = 60$ meV and (b) for different temperatures and different Fermi energies at $\mu = 2 \cdot 10^5$ cm^2/Vs for the bilayer graphene

$$+\left[\frac{\eta(z,\omega)^2\omega^2}{c^2} - k_x^2\right] H_y(z) = 0, \qquad (9)$$

$$E_x(z) = -\frac{ic}{\omega\eta(z,\omega)^2}\frac{dH_y(z)}{dz} \qquad (10)$$

with $H_y(z)\to 0$ for $z\to\pm\infty$.

For the calculations of the ac fields spatial distributions, we used values of the complex refractive indexes of Si and other materials from [9] and [10], respectively. The threshold conductivity (when gain and losses are equal) dependencies on Si layer width are shown in Fig.3b for three frequencies $\omega/2\pi = 2$, 4, and 6 THz. From Fig.3b it is clear that the minimal threshold conductivity (corresponding to an optimal Si layer width)

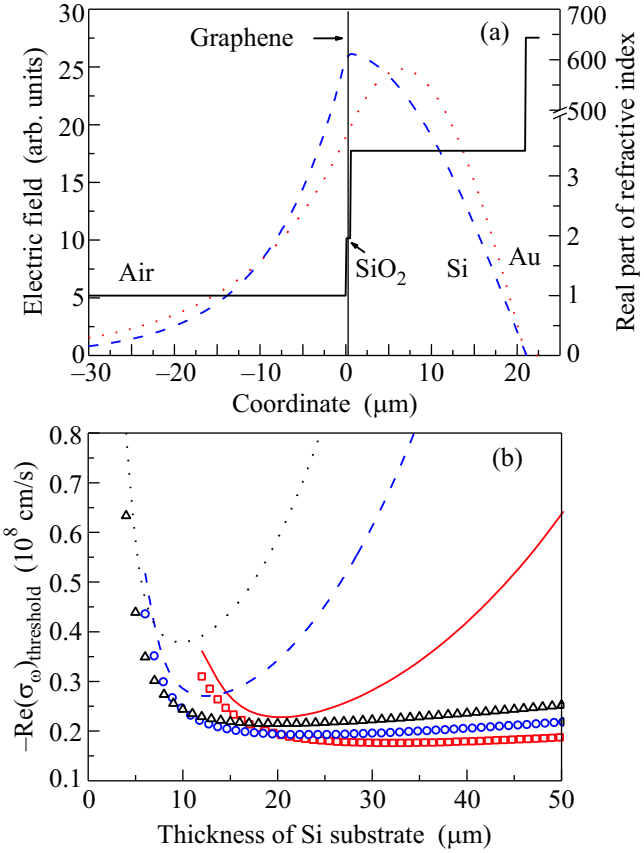

Fig.4. (a) Spatial distributions of the refractive index (solid line) and ac electric fields of TE_0 mode (dotted line) and TM_0 mode (dashed line) in waveguide for frequency 2 THz (a). Horizontal arrow indicates the graphene layer position (vertical line). (b) Dependencies of the threshold conductivity for the TE_0 and TM_0 modes on the thickness of Si substrate in this structure for frequencies $\omega/2\pi = 2$ THz ($\hbar\omega \approx 8.27$ meV, solid curve corresponds to the TE_0 mode and open squares correspond to the TM_0 mode) and $\omega/2\pi = 4$ THz ($\hbar\omega \approx 16.54$ meV, dashed curve corresponds to the TE_0 mode, open circles correspond to the TM_0 mode), $\omega/2\pi = 6$ THz ($\hbar\omega \approx 24.81$ meV, dotted curve is for the TE_0 mode whereas open triangles are for TM_0 mode)

increases with the radiation frequency growth. It is due to absorption growth in SiO_2 layers. From Fig.3b one can conclude that the absolute value of the threshold conductivity for TM_0 less than $2 \cdot 10^7$ cm/s for the frequency range $\omega/2\pi = 2$–6 THz and approximately twice greater for the TE_0 mode.

Our calculations show that the absorption coefficient of electromagnetic modes in such a waveguide is about $4\,\mathrm{cm}^{-1}$. So, as follows from Fig.3, the gain coefficient for the laser under consideration is about 10–$15\,\mathrm{cm}^{-1}$.

Let us estimate the incident optical power required to obtain $F = 60$ meV at $T = 300$ K. According to Eqs. (6) and (7), this occurs when $n \simeq 4.2 \cdot 10^{11}\,\mathrm{cm}^{-2}$ for the one layer graphene and $n \simeq 4.1 \cdot 10^{12}\,\mathrm{cm}^{-2}$ for the bilayer graphene. The required rate of photogeneration is equal to $G = n/\tau_R$, where τ_R is the recombination time. By now, there is no clear understanding of the nonradiative recombination mechanisms in graphene with relatively high electron and hole concentrations. The point is that if there is a small gap between the conduction and valence bands (due to different reasons, for instance due to a disorder) resulting in a perturbation of the linear dispersion relations, the Auger recombination with the participation of two electrons and one hole (or one electron and two holes) is forbidden due to the energy and momentum conservation. This might imply that more complex Auger processes can play an essential role in the recombination in nominally gapless graphene. Due to this, one can expect that the nonradiative recombination time is markedly longer than $\tau_R \simeq 2$ ps [11] (for the electron and hole concentrations in question). As for the radiative recombination time, the estimates yield $\tau_R \approx 400$ ns. In the most "pessimistic" case, assuming that $\tau_R \simeq 2$ ps and considering that in the waveguide structure under consideration the pumping optical radiation twice passes through graphene layer which absorbs only the portion of the incident radiation power equal to $2\pi e^2/\hbar c$, for the rate of photogeneration of the electron-hole pairs required for lasing one obtains $G = 2.1 \cdot 10^{23}\,\mathrm{cm}^{-2}\cdot\mathrm{s}^{-1}$. If the pumping is provided by CO_2 laser with the photon energy about 120 meV, the pertinent pumpimg power density should be about $4 \cdot 10^4\,\mathrm{W/cm}^2$. Analogous estimate for $F = 20$ meV at $T = 77$ K yields for the pumping power density required $1.3 \cdot 10^3\,\mathrm{W/cm}^2$. This is approximately 30 times smaller value than that in the previous estimate. Note that both these pumping powers are quite routine for pulse excitation. The threshold pumping power in the devices with the active region comprising several (but properly separated) graphene layers might be decreased correspondingly. If the dominating recombination mechanism is associated with radiative processes (most "optimistic" case), setting $\tau_R \approx 400$ ns [2], one can find that the pumping optical power required for lasing is more then five order smaller than in the above estimate. In this regard, the bilayer graphene, where the Auger recombination is forbidden due to the momentum and energy conservation, appears to be rather attractive as the active media in the lasers under consideration.

In conclusion, we considered a laser with optical pumping comprising a graphene layer or graphene bilayer as the active media and a waveguide structure. Using the developed model, it was shown that the laser under consideration on the base of realistic structure can

generate THz radiation at feasible pumping optical powers. The value of the threshold pumping optical power dramatically depends on the dominating recombination mechanism. Due to this, detailed studies of the Auger processes involving many particles and disorder are indispensable.

This work was in part financially supported by the Program of Russian Academy of Sciences "Coherent optical radiation of semiconductor compounds and structures" (Contract # 02.518.11.7031), Russia. The work at University of Aizu was supported by the Japan Science and Technology Agency, CREST, Japan.

1. V. Ryzhii, M. Ryzhii, and T. Otsuji, J. Appl. Phys. **101**, 083114 (2007).
2. A. Satou, F. T. Vasko, and V. Ryzhii, Phys. Rev. B **78**, 11531 (2008).
3. F. Rana, IEEE Trans. Nanotechnol. **7**, 91 (2008).
4. V. Ryzhii, M. Ryzhii, and T. Otsuji, Phys. Stat. Sol. (c) **5**, 261 (2008).
5. M. Suemitsu, Y. Miyamoto, H. Kanda, and A. Konno, *Proc. 14th Int. Conf. on Solid Films and Surfaces (ICSFS-14)*, Dublin, 2008; e-Journal of Surf. Sci. and Nanotechnol. (to be published).
6. E. McCann and V. Fal'ko, Phys. Rev. Lett. **96**, 086805 (2006).
7. S. V. Morozov, K. S. Novoselov, M. I. Katsnelson et al., Phys. Rev. Lett. **100**, 016602 (2007).
8. Y.-W. Tan, Y. Zhang, K. Bolotin et al., Phys. Rev. Lett. **99**, 246803 (2007).
9. A. Dargys and J. Kundrotas, *Handbook on Physical Properties of Ge, Si, GaAs, and InP*, Science and Encyclopedia Publishers, Vilnius, 1994.
10. F. Rana, Phys. Rev. B **76**, 155431 (2007).
11. E. D. Palik, *Handbook of Optical Constants of Solids*, Academic Press, New York, 1998.